Title
Regional transcriptional architecture of Parkinson's disease pathogenesis and network spread

Journal
Brain, 142(10)

ISSN
0006-8950

Authors
Freeze, Benjamin
Pandya, Sneha
Zeighami, Yashar
et al.

Publication Date
2019-10-01

DOI
10.1093/brain/awz223

Peer reviewed

doi:10.1093/brain/awz223 BRAIN 2019: 0; 1–14 | 1

BRAIN
A JOURNAL OF NEUROLOGY

Regional transcriptional architecture of Parkinson's disease pathogenesis and network spread

Benjamin Freeze,[1] Sneha Pandya,[1] Yashar Zeighami[2] and Ashish Raj[1,3]

Although a significant genetic contribution to the risk of developing sporadic Parkinson's disease has been well described, the relationship between local genetic factors, pathogenesis, and subsequent spread of pathology throughout the brain has been largely unexplained in humans. To address this question, we use network diffusion modelling to infer probable pathology seed regions and patterns of disease spread from MRI atrophy maps derived from 232 *de novo* subjects in the Parkinson's Progression Markers Initiative study. Allen Brain Atlas regional transcriptional profiles of 67 Parkinson's disease risk factor genes were mapped to the inferred seed regions to determine the local influence of genetic risk factors. We used hierarchical clustering and L_1 regularized regression analysis to show that transcriptional profiles of immune-related and lysosomal risk factor genes predict seed region location and the pattern of disease propagation from the most likely seed region, substantia nigra. By leveraging recent advances in transcriptomics, we show that regional microglial abundance quantified by high fidelity gene expression also predicts seed region location. These findings suggest that early disease sites are genetically susceptible to dysfunctional lysosomal α-synuclein processing and microglia-mediated neuroinflammation, which may initiate the disease process and contribute to spread of pathology along neural connectivity pathways.

1 Department of Radiology, NewYork-Presbyterian Hospital/Weill Cornell Medicine, New York, USA
2 McConnell Brain Imaging Centre, Montreal Neurological Institute, McGill University
3 Department of Radiology and Biomedical Imaging, University of California, San Francisco

Correspondence to: Benjamin Freeze
Massachusetts General Hospital
Harvard Medical School
Department of Radiology
55 Fruit St.
Boston, MA 02114, USA
E-mail: bfreeze@mgh.harvard.edu

Keywords: Parkinson's disease; α-synuclein; microglia; neuroinflammation; lysosome

Abbreviations: NDM = network diffusion modelling; SR = seed region likelihood

Introduction

Parkinson's disease is the second most common neurodegenerative disease (Kowal *et al.*, 2013), causing devastating motor, neuropsychiatric and visuospatial dysfunction (Chaudhuri *et al.*, 2006). Numerous genetic factors have been linked to both hereditary and sporadic forms of Parkinson's disease, but the role of genetics in initiating region-specific pathology and controlling spread of disease across brain regions is poorly understood. Recent work has identified a role for genes involved in trans-synaptic transfer of α-synuclein in influencing the regional pattern of

Received January 31, 2019. Revised April 4, 2019. Accepted May 28, 2019

brain atrophy (Freeze *et al.*, 2018) but because of experimental limitations in humans, most work in this area has been limited to animal models (Mao *et al.*, 2016). A better understanding of how genetic factors contribute to the region-specific risk of developing Parkinson's disease pathology is crucial to identify promising genetic pathways for therapeutic intervention.

In humans, MRI-derived regional brain atrophy is an experimentally accessible measure of local pathology *in vivo*. Both cortical and subcortical brain regions have been shown to exhibit atrophy in Parkinson's disease (Tinaz *et al.*, 2011; Jia *et al.*, 2015; Yau *et al.*, 2018), including basal ganglia regions that contribute to cardinal motor symptoms. Multiple lines of evidence have suggested that pathology propagates from a small number of early disease sites along neural connectivity pathways (Desplats *et al.*, 2009; Luk *et al.*, 2012), ultimately affecting most of the brain. Previous work using network diffusion modelling (NDM) has shown that this process can be described by considering the spread of pathology as a diffusion process on the structural connectome (Raj *et al.*, 2012; Pandya *et al.*, 2019), with grey matter atrophy serving as a measure of local pathology. By seeding NDM pathology at every possible brain region, and comparing NDM predictions of atrophy with the true atrophy map, the regional origin of pathology can be inferred (Torok *et al.*, 2018; Pandya *et al.*, 2019). In Parkinson's disease, NDM predicts that likely seed regions are located in the midbrain and other subcortical regions, with substantia nigra representing the most likely seed region (Pandya *et al.*, 2019).

Here we ask whether regional transcriptional profiles of Parkinson's disease risk factor genes can predict the pathology seed region and pattern of spread derived from the atrophy map and NDM. Genes that predict the regional origin of pathology may represent therapeutic targets that are particularly important in the early disease process and may therefore be more likely to significantly affect disease progression. We find that transcriptional profiles of immune-related and lysosomal Parkinson's disease risk factor genes predict the pathology seed region, as well as the pattern of early disease spread. By exploiting recent advances in transcriptomics (Kelley *et al.*, 2018), we also show that regional microglial abundance predicts the regional origin of pathology, suggesting that vulnerable regions may be susceptible to microglial-mediated pathology in the early disease state.

Materials and methods

Parkinson's disease regional atrophy

The regional Parkinson's disease atrophy map was calculated as in Zeighami *et al.* (2015). Briefly, high resolution T_1-weighted MRIs were obtained from the prospective multicentre Parkinson's Progression Markers Initiative (PPMI, ClinicalTrials.gov identifier: NCT0114102; Marek *et al.*, 2011) for healthy control subjects ($n = 117$ total; $n = 74$ male, $n = 43$ female; mean age 59.7 years) and *de novo* Parkinson's disease subjects ($n = 232$ total; $n = 155$ male, $n = 77$ female; mean age 61.2 years) enrolled between 2010 and 2013. Informed consent and Institutional Review Board approval were obtained, and HIPAA (Health Insurance Portability and Accountability Act) compliance was maintained. Additional study information is available at www.ppmi-info.org. Images were pre processed, which included normalization, correction of intensity non-uniformity and denoising. Following linear and non linear registration to the MNI-ICBM 152 template, regional atrophy was calculated for each region in a 112 region parcellation using deformation-based morphometry (Ashburner *et al.*, 1998). Resultant atrophy was re-scaled with regional atrophy represented as a z-score. Thirty-four cerebellar regions were excluded, and further analysis was performed on the remaining 78 cortical and subcortical regions.

Connectome construction

Structural connectivity was derived from high resolution diffusion-weighted MRI from the IIT Human Brain Atlas v.3 ($n = 72$ healthy control subjects). Connectivity between two grey matter regions was defined as: anatomical connection density (ACD) – the fraction of superficial connected nodes with respect to total number of superficial nodes (Iturria-Medina *et al.*, 2007). The connectivity matrix $C = \{c_{i,j}\}$ is defined as all pairwise values of ACD such that $c_{i,j}$ represents the connection strength of white matter fibre pathways between the i^{th} and j^{th} grey matter regions. This measure intrinsically corrects for variation in brain size as raw connection strength is divided by the sum of region-pair surface areas. Bidirectional connections are assumed (Pandya *et al.*, 2019).

Network diffusion modelling

Parkinson's disease progression is considered as a diffusion process on the connectivity matrix C (Raj *et al.*, 2012). A detailed description of Parkinson's disease progression as predicted by NDM is available in Pandya *et al.* (2019). Briefly, the transmission of pathology from region 1 to region 2 is asserted to satisfy the equation

$$\frac{dx_1}{dt} = \beta c_{1,2}(x_2 - x_1) \quad (1)$$

where x_1 and x_2 are pathology concentrations in each region, and β is a global diffusivity constant. Extending this relationship to all regions i we define the regional pathology vector $x(t) = \{x_i(t)\}$, and the above equation become: $\frac{dx(t)}{dt} = -\beta H x(t)$, where H is the graph Laplacian $H = I - D^{-\frac{1}{2}} C D^{-\frac{1}{2}}$.

The regional atrophy vector x at time point t may then be adequately modelled by the equation $x(t) = e^{(-\beta H t)} x_0$ where x_0 is the initial state of the model at $t = 0$ (e.g. initial atrophy or pathological insult). As in Pandya *et al.* (2019), the NDM was separately initialized at all possible seed regions such that x_0 is 1 at each of the bilateral seed regions (e.g. left and right substantia nigra) and 0 at all other regions. The Pearson correlation coefficient (R) of the actual measured atrophy map with the NDM-predicted regional atrophy vector $x(t)$ was calculated for each timepoint t and for each seed region. The

maximum R occurring over all model time points t for each seed region was determined and is considered a measure of seed region likelihood (SR). Following model initialization, we also calculate arrival time for each non-seed region, defined as the time t at which 98% of the maximum theoretical $x(t)$ value in that region is achieved. As SR approaches zero for unlikely seed regions, the top 20 bilateral seed regions were considered for joint regional transcriptional analysis. Similarly the top 20 arrival time regions were analysed to capture the pattern of early pathology spread.

Regional transcriptional analysis

Sixty-seven putative Parkinson's disease risk factor genes from the recent Parkinson's disease genome-wide association study (GWAS) meta-analysis by Chang *et al.* (2017) were identified for regional transcriptional analysis. For each gene, data were obtained from the publicly available human Allen Brain Atlas (ABA) (Hawrylycz *et al.*, 2012). Human ABA data for the listed gene '*CDC71*' could not be located. The ABA includes 926 brain regions, with each region having microarray expression levels from a set of 58 692 probes that correspond to 29 181 distinct genes. All ABA regions were mapped to the same 78 region atlas used for NDM. Semantic matching was used as the initial mapping strategy for all regions (i.e. ABA samples mapping to 'hippocampus' on the ABA atlas are mapped to 'hippocampus' in the 78 region parcellation used in this study). In cases for which semantic matching could not be used because of differences in region demarcation, atlases were visually compared, and ABA samples were mapped to the closest corresponding grey matter region in our 78 region parcellation. ABA samples spanning more than one region in our 78 region parcellation were excluded from analysis. All samples for all probes within the same region were then averaged for each gene. White matter tracts were excluded from analysis. Expression for each gene was averaged for six subject brains (which comprises data for six left hemispheres and two right hemispheres; more information can be found at help.brain-map.org/download/attachments/2818165/Normalization_WhitePaper.pdf). The top 10 high differential stability genes as in Hawrylycz *et al.* (2015), and the top five microglial and neuronal high fidelity genes as in Kelley *et al.* (2018) were mapped in the same way.

Gene functional classification

Lysosomal, mitochondrial and autophagy-related genes were initially classified as described previously (Chang *et al.*, 2017). Immune-related genes were initially classified according to the ImmPort database (Bhattacharya *et al.*, 2018). Gene classification was manually reviewed, and additional genes were added to the relevant functional class in cases in which literature evidence supports a role in the class.

Hierarchical clustering of regional transcription

Unweighted pair group method with arithmetic mean (UPGMA) agglomerative hierarchical clustering of expression data across genes and regions was performed using the MATLAB routine *clustergram* (Bar-Joseph *et al.*, 2001). The Euclidean distance metric was used. Colour maps were defined using the *morgenstemning* function (M. Geissbuelher).

L_1 regularized regression analysis

L_1 regularized regression was performed using the MATLAB routine *lasso* (Tibshirani, 2011). Five-fold cross-validation was used in all cases. Display of regression coefficient and mean squared error (MSE) curves was performed using the routine *lassoplot*.

Permutation analysis

Genetic expression values were permuted across brain regions 10^4 times for each tested gene set as described in the 'Results' section. Correlation coefficients for average permuted gene class expression and either SR or arrival time were then calculated. Cumulative probability curves were created using the MATLAB routine *cdfplot*.

Data availability

All data used in this study will be made available upon reasonable request.

Results

Network diffusion modelling of Parkinson's disease pathology

Previous work used NDM as a mechanistic framework to dissect Parkinson's disease pathogenesis and network propagation of pathology. In this context, brain region-specific pathology is considered to be indirectly but adequately measurable from the far more accessible surrogate measure of a deformation based morphometry (DBM) atrophy map, which is derived from T_1-weighted volumetric MRI studies from 232 PPMI Parkinson's disease and 117 healthy control subjects (Zeighami *et al.*, 2015). Spread of pathology occurs via neural pathways, which are defined by diffusion MRI-derived structural connectivity. As in a recent article by Pandya *et al.*, NDM was employed using each region in the atlas as an initial pathology seed and the likelihood of each seed was quantified by the correlation of the NDM regional atrophy prediction with the true atrophy map (Pandya *et al.*, 2019). As every atlas region is simulated as a seed region, this method makes no *a priori* assumptions about the importance of seeds; and the correlation of the NDM prediction with the atrophy map (referred to as seed region likelihood) thereby represents an unbiased estimate of the propensity of each seed to explain the atrophy map.

Using this approach, the substantia nigra was determined to be the most likely seed region (SR = 0.65). Figure 1 illustrates the process by which the NDM prediction for substantia nigra seeding was derived and the similarity of

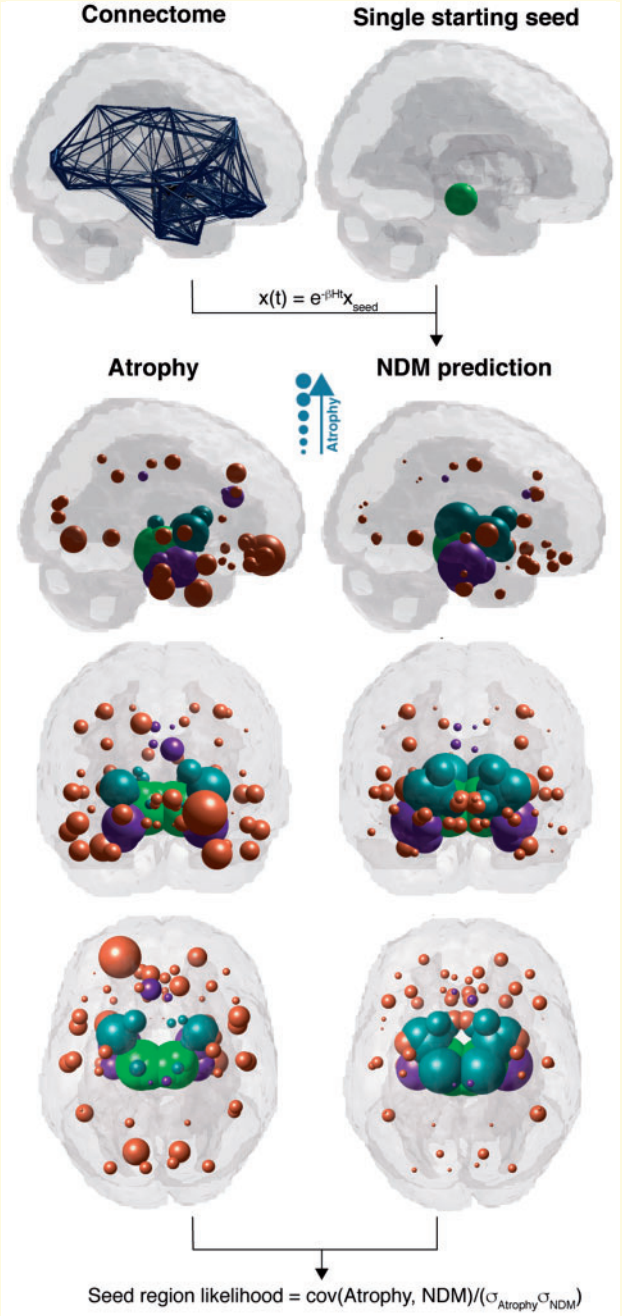

Figure 1 Network diffusion modeling predictions of Parkinson's disease atrophy, pathology seed region, and spread pattern. Schematic of the network diffusion modeling approach using the top seed substantia nigra as an example. *Top*: Interregional connectivity and a single seed at the substantia nigra are used to initialize the network diffusion model. *Bottom*: Triplanar glassbrain comparisons of the atrophy map and NDM predictions. The radius of the sphere centred on each brain region is proportional to atrophy. See Tables 1 and 2 for seed region likelihood and arrival time at each brain region, respectively.

the substantia nigra-seeded NDM prediction to the atrophy map, which demonstrates extensive involvement of subcortical brain regions. The top 20 seed regions with the most accurate atrophy predictions as quantified by SR are shown in Table 1. Top seed regions tend to be very atrophic, suggesting that the role as an early disease site also allows for time-dependent accumulation of cellular pathology, dysfunction, and atrophy. However, there are regions such as putamen, which despite being more atrophic than subthalamic nucleus (atrophy z-score of 2.8 versus 2.0), is a much poorer seed region (SR 0.30 versus 0.53), which demonstrates the crucial role of interregional connectivity in determining SR. The spread of pathology from the most likely substantia nigra seed to subsequent regions can be quantified by arrival time, which is defined as the time to achieve 98% of the maximum atrophy. The top 20 regions with the smallest arrival times from the substantia nigra seed are also shown (Table 2). In accordance with actual atrophy progression, NDM predicts that early pathology spreads from the substantia nigra to connected subcortical regions in the basal ganglia and limbic system.

Table 1 Best fit atrophy map correlation coefficient (seed region likelihood) for NDM predicted atrophy seeded at each brain region

Region	SR (R)	Atrophy (z)
Substantia nigra	0.65	4.1
Red nucleus	0.58	3.0
Amygdala	0.56	3.2
Subthalamic nucleus	0.53	2.0
Parahippocampal gyrus	0.44	1.9
Hippocampus	0.44	1.5
Anterior middle temporal lobe	0.37	1.4
Lateral occipitotemporal gyrus	0.37	1.0
Anterior inferolateral temporal lobe	0.35	1.0
Anterior superior temporal gyrus	0.34	1.0
Inferior middle temporal gyrus	0.32	1.0
Putamen	0.30	2.8
Thalamus	0.30	0.6
Pallidum	0.28	1.1
Superior central temporal gyrus	0.27	0.8
Insula	0.24	0.5
Nucleus accumbens	0.24	−0.4
Subcallosal area	0.24	−2.6
Anterior orbital gyrus	0.24	2.1
Caudate nucleus	0.24	0.7

R is shown for NDM seeded at the top 20 bilateral regions. Average atrophy (z-score) is also shown for the top 20 seed regions.

Increased transcription of Parkinson's disease risk factor genes in early disease sites

The set of putative Parkinson's disease risk factor genes from the recent Chang *et al.* (2017) GWAS meta-analysis was mapped to the same atlas as that used for network diffusion analysis. Hierarchical clustering was performed across all genes ($n = 67$) and brain regions ($n = 39$ bilateral

Table 2 Top 20 arrival time regions for NDM seeded at the top seed region, substantia nigra

Region	Arrival time, substantia nigra (AU)
Red nucleus, R	10.1
Red nucleus, L	12.1
Subthalamic nucleus, L	12.1
Subthalamic nucleus, R	12.1
Parahippocampal gyrus, R	14.1
Pallidum, R	14.1
Hippocampus, R	16.1
Parahippocampal gyrus, L	18.1
Thalamus, L	18.1
Hippocampus, L	20.2
Amygdala, L	20.2
Thalamus, R	20.2
Nucleus accumbens, R	24.2
Putamen, R	24.2
Pallidum, L	24.2
Amygdala, R	28.2
Caudate nucleus, R	28.2
Nucleus accumbens, L	28.2
Subcallosal area, R	28.2
Caudate nucleus, L	32.3

Smaller arrival times reflect earlier involvement in Parkinson disease pathology.
AU = arbitrary units; L = left; R = right.

averaged regions) to determine whether discrete patterns of transcript abundance are present. The resultant dendrogram is shown in Fig. 2A. A striking pattern of differential expression of Parkinson's disease genes is observed, with largely reversed patterns of transcription between primarily subcortical regions (left) and cortical regions (right). At the top level of region clustering (two clusters), one cluster contains only five brain regions, while the other contains 34 regions. Despite containing only five regions, the first cluster is composed of subcortical regions with SR rank 1 (substantia nigra), 2 (red nucleus) and 4 (subthalamic nucleus), suggesting that there is a relationship between expression of Parkinson's disease genes and likelihood of a region representing an initiation site for pathology as inferred by NDM. A similar observation is made when considering the arrival time of pathology to other regions from the top ranked substantia nigra seed. The same five-region cluster is composed of the substantia nigra seed itself, and regions with arrival time rank 1 (red nucleus), 2 (subthalamic nucleus) and 4 (pallidum). The remaining 34-region cluster contains only two of the top five NDM seeds and two of the top five arrival time regions, despite containing more than 6-fold more brain regions. This regional distribution of top seed regions and top arrival time regions is unlikely to be due to chance (Fisher's exact test, $P = 0.01$ in both cases). Further inspection of the larger 34 region cluster reveals that it is composed of a five-region cluster including the limbic system structures amygdala (seed rank 3) and hippocampus (arrival time rank 5). The larger 29-region cluster primarily contains unranked cortical structures, with the exception of the parahippocampal gyrus (seed rank 5, arrival time rank 3). As expected from visual inspection of the dendrogram, top five seed regions exhibit significantly more upregulated and downregulated genes than all other regions, with relatively more upregulated genes (Fig. 2B).

Expression of immune-related and lysosomal gene classes predicts pathology seed region

Consistent with the overall pattern of gene expression visualized in Fig. 2A, average expression across all 67 Parkinson's disease-related genes is positively correlated with SR (n = top 20 bilateral NDM seed regions; $r = 0.36$, $P = 0.02$; Fig. 3A). As a control, we performed a similar analysis using the expression of the top 10 high differential stability genes (Hawrylycz *et al.*, 2015). These genes have differential regional expression patterns that are highly conserved across individuals. In contrast to the Parkinson's disease risk factor genes, average expression of high differential stability genes is not significantly correlated with SR, demonstrating that this effect is not a general feature of transcription in high likelihood seed regions ($r = -0.30$, $P = 0.059$, Supplementary Fig. 1).

The set of Parkinson's disease risk factor genes was subsequently subdivided according to functional classes implicated in Parkinson's disease: immune-related, lysosomal, autophagy-related, and mitochondrial. Average expression of immune-related genes is highly correlated with SR (Fig. 3B, $r = 0.72$, $P = 3.5 \times 10^{-4}$), while average lysosomal gene expression demonstrates correlation similar to that of the Parkinson's disease gene set as a whole (Fig. 3C, $r = 0.40$, $P = 0.01$). Average expression of autophagy-related and mitochondrial genes was not correlated with SR (Fig. 3D and E). Interestingly, expression of *SNCA*, which encodes α-synuclein, is also uncorrelated with SR ($r = -0.14$, $P = 0.38$, Supplementary Fig. 2).

To determine whether the observed significant correlation coefficients were likely to be observed because of random structure within the set of gene expression values, we performed 10^4 permutations of expression values across brain regions and calculated the resultant correlation coefficients for SR and average permuted gene expression. As shown in Fig. 3F, the actual correlation coefficients obtained for the entire gene set, and the lysosomal and immune-related gene subsets, are located in the rightmost region of the cumulative probability curve, distant from the mean r of ~0 for permuted datasets. Together, these results suggest that likely seed regions are enriched in transcripts for Parkinson's disease risk factor genes, and that immune-related and lysosomal genes are specifically related to this effect.

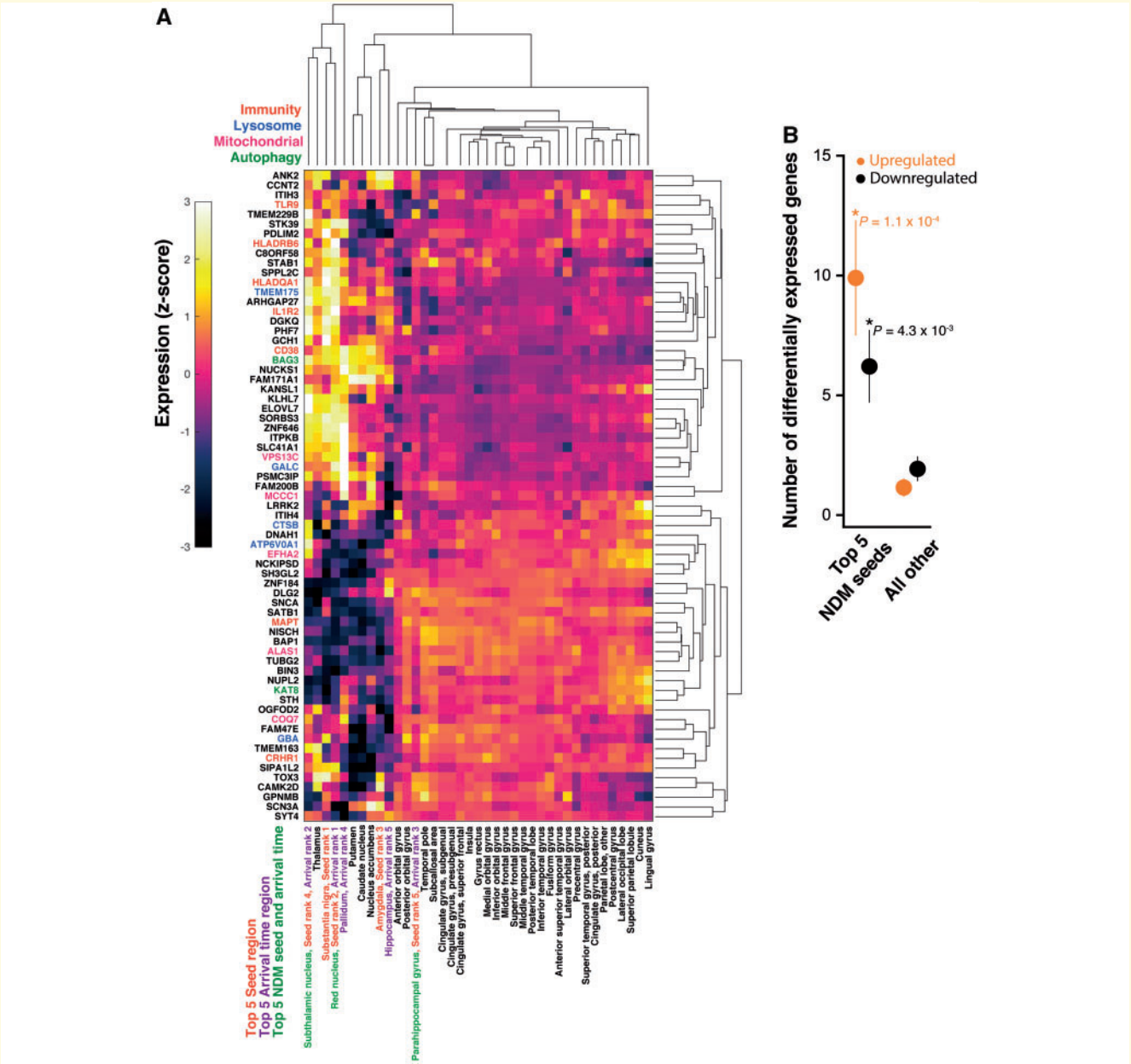

Figure 2 Hierarchical clustering of Parkinson's disease risk factor regional transcription. (**A**) Hierarchical clustering of regional transcript abundance of 67 GWAS Parkinson's disease risk factor genes. Clustering was performed for both regions (n = 39 bilateral averaged regions) and genes. Gene functional class (immunity, lysosome, mitochondrial and autophagy) is colour-coded. Top five seed, top five arrival time, and top five seed and arrival time, regions are colour-coded. Top seed and arrival time regions demonstrate similar expression patterns, and cluster together along the left aspect of the region axis. (**B**) Average number of differentially expressed genes for top five seed regions (*left*) and all other regions (*right*). Top seed regions demonstrate significantly more upregulated and downregulated genes (z-score threshold of ± 2), with relatively more upregulated genes.

Transcription of specific lysosomal and immune-related genes predicts pathology seed region

To determine whether transcriptional profiles of individual lysosomal genes predict SR we performed cross-validated L_1 regularized regression with expression profiles of the classified lysosomal genes as independent variables and SR as the dependent variable. At the value of the tuning parameter λ commonly used to choose a sparse regression model [i.e. that which achieves a MSE one standard error larger than that for the minimum MSE (Hastie, 2015)], coefficients for GBA and TMEM175 expression profiles remain non-zero, indicating that these are the most important predictor variables (Fig. 3G). The remaining expression

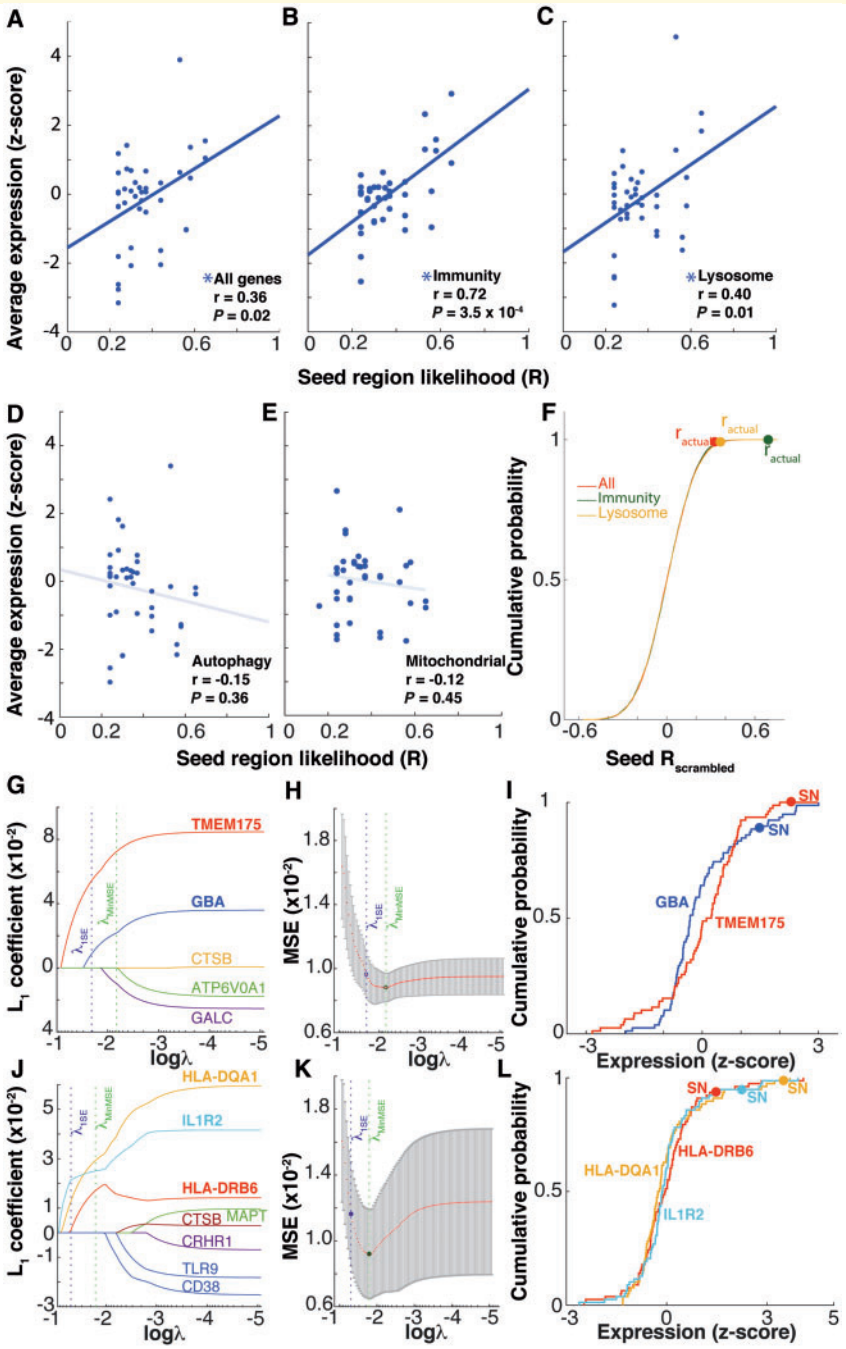

Figure 3 Prediction of seed region by immune-related and lysosomal gene transcription. (**A**–**E**) Scatterplots of seed region likelihood (R) and average regional expression (n = top 20 bilateral seed regions) across gene classes. Expression across all Parkinson's disease-risk factor genes (n = 67) (**A**), as well as immune-related (n = 8) (**B**) and lysosomal (n = 5) (**C**) subsets is positively correlated with SR. Autophagy-related gene expression (n = 3) (**D**) and mitochondrial gene (n = 5) (**E**) expression is not significantly correlated with SR. (**F**) Cumulative probability distributions of correlation coefficients for expression and SR (Seed $R_{scrambled}$) obtained by permutation of expression values across regions ($n = 10^4$ permutations per tested gene class). (**G** and **J**) Cross-validated L_1 regularized regression coefficient curves for individual lysosomal (**G**) and immune-related (**J**) gene expression plotted against the logarithm of the tuning parameter λ. Genes that maintain non-zero coefficients at the value of λ one standard error greater than the value of λ that achieves minimum cross-validation MSE are considered important predictor variables for SR. Lysosomal genes *GBA* and *TMEM175*; and immune-related genes *HLA-DQA1*, *IL1R2* and *HLA-DRB6* are important predictor variables. (**H** and **K**) Mean squared error (MSE) curves corresponding to coefficient curves in (**G**) and (**J**), respectively. (**I** and **L**) Cumulative probability curves for regional expression of important lysosomal (**I**) and immune-related (**L**) predictor genes. Each gene is highly expressed in the top seed region, substantia nigra, as indicated on the curve.

profile coefficients for *GALC*, *CTSB*, and *ATP6V0A1* are zero at this value of λ. Analysis of the distribution of these genes across all brain regions shows that *GBA* and *TMEM175* are highly expressed in substantia nigra (Fig. 3I), compatible with a causal role for lysosomal dysfunction in Parkinson's disease pathogenesis in the most likely seed region. We performed a similar L_1 regularized regression analysis for the set of immune-related genes. Notably, transcriptional profiles of two major histocompatibility complex class II genes, *HLA-DQA1* and *HLA-DRB6*, are important predictors of pathology seed region. The other important predictor gene is *IL1R2*, a complex regulator of IL1 signalling (Fig. 3J). These genes are also highly expressed in substantia nigra (Fig. 3L).

Enrichment in risk factor transcripts is uncorrelated with the overall atrophy pattern

Although SR is correlated with regional atrophy (r = 0.70, $P = 4.0 \times 10^{-7}$, Fig. 4A), average expression across all Parkinson's disease genes is not correlated with the magnitude of atrophy across top seed regions (Fig. 4B, $n = 40$ regions for top 20 bilateral NDM seeds, r = 0.08, $P = 0.61$) or across all regions in the full brain parcellation (Fig. 4C, $n = 78$ regions, r = 0.07, $P = 0.56$). This result suggests that enrichment in Parkinson's disease-risk factor transcripts is more related to disease initiation than control of the overall regional atrophy pattern.

Transcription of immune-related and lysosomal genes predicts the early pattern of spread from the substantia nigra

We next sought to determine whether Parkinson's disease risk factor transcription also predicts the pattern of pathology spread from substantia nigra, the most likely seed region. To this end, we calculated the correlation between regional average transcript abundance and NDM-predicted arrival time from substantia nigra (defined as the model time needed to achieve 98% of the maximum theoretical $x(t)$ at that region, after seeding x_0 at the substantia nigra only) across regions. Given that pathology originates in the substantia nigra in this model, the substantia nigra itself has arrival time 0 by definition. Arrival times for subsequently affected brain regions become progressively greater as regions achieve near maximal $x(t)$. Average transcription of all genes is negatively correlated with arrival time (Fig. 5A, r = −0.62, $P = 3.5 \times 10^{-3}$, $n = 20$ smallest arrival time regions, excluding substantia nigra itself) suggesting that regions most likely to be affected early in the disease process are enriched in Parkinson's disease risk factor transcripts. Expression of immune-related and lysosomal genes is negatively correlated with arrival time (r = −0.73, $P = 2.6 \times 10^{-4}$; and r = −0.59, $P = 5.7 \times 10^{-3}$, respectively), while expression of autophagy-related and mitochondrial genes is not significantly correlated with arrival time (Fig. 5B–E). L_1 regularized regression analysis was again used to determine whether important lysosomal and immune-related genetic predictors of the spread pattern from substantia nigra overlap with those predictive of the pathology seed region. Indeed, all of the genes identified as predictive of the seed region were also identified as predictive of the early spread pattern as quantified by arrival time. Other genes were also identified as important predictors, including the lysosomal gene *ATP6V0A1* and multiple immune-related genes including *CRHR1* and *MAPT* (which encodes tau) (Fig. 5G–J).

Microglial abundance predicts seed region location

We observed that several of the immune-related genes identified as important predictors of the seed region and early

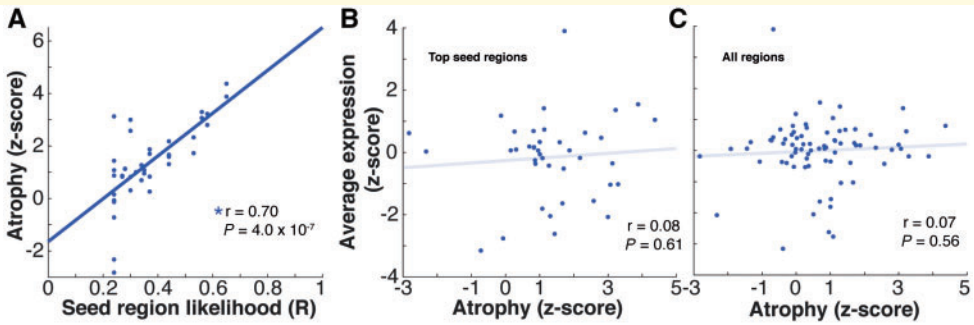

Figure 4 Regional transcription of Parkinson's disease risk factor genes does not predict the overall atrophy pattern. (**A**) Scatterplot of SR and regional atrophy (n = top 20 bilateral seed regions), showing positive correlation. (**B**) Scatterplot of regional atrophy and average Parkinson's disease risk factor gene expression for top seed regions, demonstrating absence of significant correlation. (**C**) Regional atrophy and average Parkinson's disease risk factor gene expression are also uncorrelated across all regions, including top seed and non-top seed regions (n = 78).

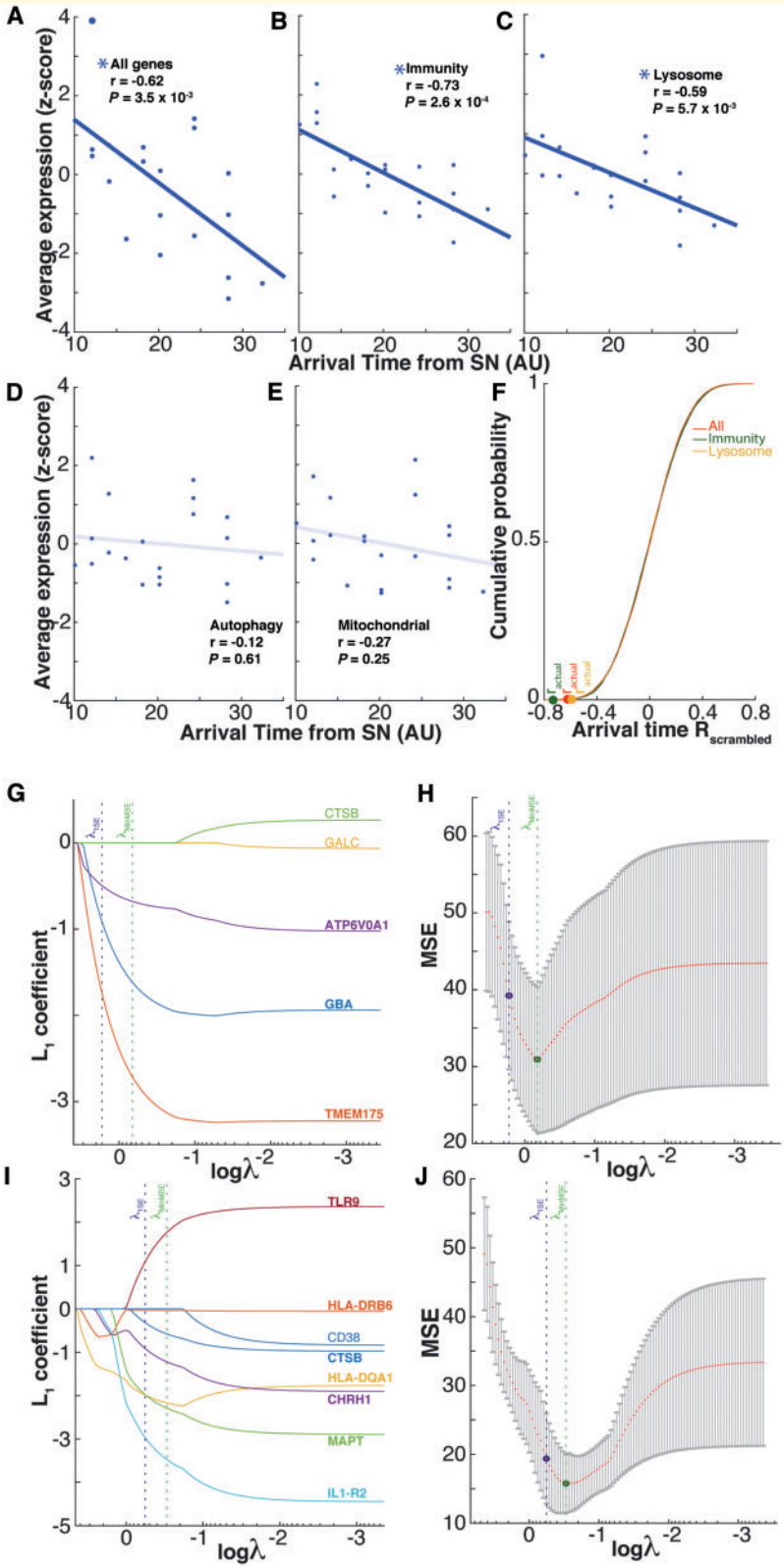

Figure 5 Prediction of spread pattern by regional transcription of immune-related and lysosomal genes. (**A**–**E**) Scatterplots of NDM arrival time from top seed region substantia nigra and average regional expression (n = top 20 bilateral seed regions) across gene classes. Expression across all Parkinson's disease-risk factor genes (n = 67) (**A**), as well as immune-related (n = 8) (**B**) and lysosomal (n = 5) (**C**) subsets is positively correlated with arrival time. Autophagy-related gene expression (n = 3) (**D**) and mitochondrial gene (n = 5) (**E**) expression is not significantly correlated with arrival time. (**F**) Cumulative probability distributions of correlation coefficients for expression and arrival time (Arrival time $R_{scrambled}$) obtained by permutation of expression values across regions ($n = 10^4$ permutations per tested gene class). (**G** and **I**) Cross-validated L_1 regularized regression coefficient curves for individual lysosomal (**G**) and immune-related (**I**) gene expression plotted against the logarithm of the tuning parameter λ. Important predictor variables have non-zero coefficients at λ one standard error from that achieving minimum MSE. (**H** and **J**) Mean squared error (MSE) curves corresponding to coefficient curves in (**G**) and (**I**), respectively.

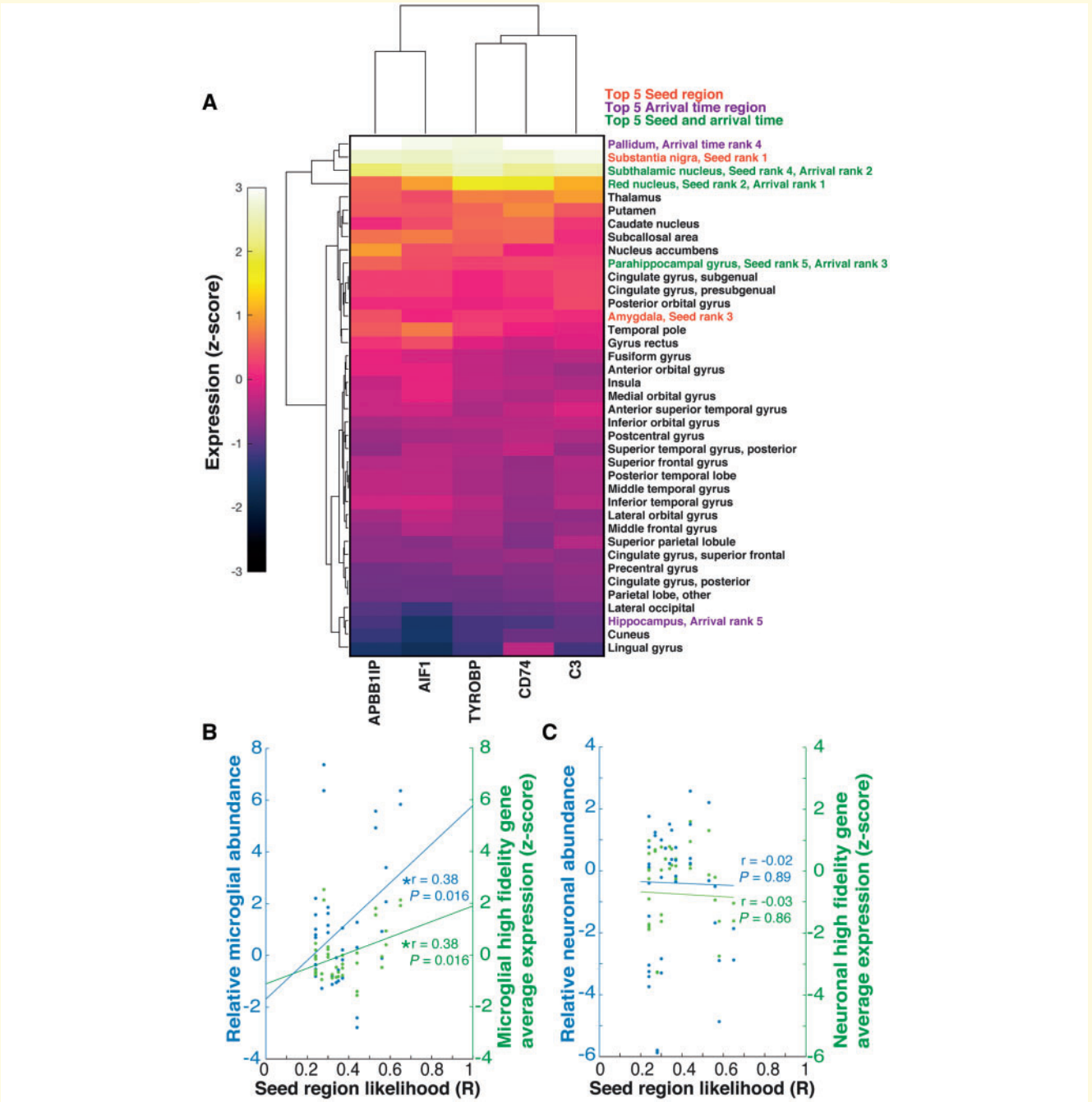

Figure 6 Microglial abundance predicts seed region location. (**A**) Hierarchical dendrogram with expression (transcript abundance) of the top five microglial high fidelity genes, clustered by both region (n = 39 bilateral averaged regions) and gene. Top seed regions cluster together at high expression values. (**B**) Scatterplot of relative microglial abundance (quantified by the first principal component of high fidelity gene expression) versus SR (n = top 20 bilateral seed regions). Relative microglial abundance is positively correlated with SR. Average microglial high fidelity gene expression is similarly positively correlated with SR. (**C**) Scatterplots of relative neuronal abundance and average neuronal high fidelity gene expression demonstrate that neither measure is correlated with SR.

pattern of spread are selectively expressed by microglia, such as HLA-DQA1. Recent work has identified genes with regional transcriptional levels highly predictive of the regional abundance of the cell type. The first principal component of regional expression of even a small number of such 'high-fidelity genes' is nearly perfectly correlated ($r > 0.99$) with regional cell type abundance (Kelley *et al.*, 2018). To determine whether regional microglial abundance predicts pathology seed region and pattern of spread, we mapped expression of the top five high fidelity microglial genes to the same 78 region atlas used before. Similar to our analysis of all Parkinson's disease risk factor genes,

hierarchical clustering was applied to regional expression of the top five high fidelity microglial genes. At the top level of clustering (two clusters), a four-region cluster was identified that contained the regions with highest expression of the microglial high-fidelity genes (Fig. 6A). This region contained the pallidum, substantia nigra, subthalamic nucleus, and red nucleus. Three of the top five seed regions and three of the top five arrival time regions were represented in this cluster. The remaining 35-region cluster contained only two each of the top seed and arrival time regions. Enrichment of top five seed regions and arrival time regions is unlikely to be due to chance (Fisher exact test, $P = 4.2 \times 10^{-3}$).

Given the correspondence between high fidelity gene expression and cell type abundance, we computed the first principal component (PC1) of high fidelity gene expression as a proxy measure of regional microglial abundance (Kelley *et al.*, 2018). Interestingly, microglial abundance was significantly correlated with SR (Fig. 6B, $r = 0.38$, $P = 0.016$), suggesting that regions enriched in microglia at baseline may be more susceptible to neuroinflammatory processes. Average expression was equally correlated with SR ($r = 0.38$, $P = 0.016$), with similarity between average expression and PC1 driven by highly correlated expression across these genes. A trend towards a negative correlation between microglial abundance and arrival time from the substantia nigra seed was not statistically significant ($r = -0.34$, $P = 0.14$). As a control, we calculated the correlation between PC1 of the top five neuronal high fidelity genes (*NSF*, *SNAP25*, *TRIM37*, *APT2A2*, and *MAPK9*) and SR. There was no correlation between these measures (Fig. 6C, $r = -0.02$, $P = 0.89$), suggesting that neuronal abundance is unrelated to Parkinson's disease pathology initiation. Similarly, average neuronal high fidelity average expression was also uncorrelated ($r = -0.03$, $P = 0.86$).

Discussion

Despite great effort investigating the genetic features of Parkinson's disease, the role of risk factor genes in determining sites of Parkinson's disease pathogenesis and patterns of spread remains largely unknown in humans. Here we have uncovered some of the molecular mediators of Parkinson's disease seeding propensity and quantify, for the first time, the contribution of innate molecular factors in mediating the regional vulnerability of certain brain regions to act as pathology seeding loci. By combining state of the art neuroimaging, computational modelling and transcriptional analysis we show that likely Parkinson's disease initiation sites are enriched in risk factor transcripts, specifically related to immune and lysosomal function. High levels of expression in seed regions may make them more susceptible to the effects of genetic variation, thereby explaining the increased risk for developing Parkinson's disease observed in GWAS studies. As we specifically examined genetic expression in healthy subjects, this suggests that there is a pattern of regional genetic vulnerability which promotes early Parkinson's disease pathology in the presence of an inciting event.

Transcriptional profiles of lysosomal genes *GBA* and *TMEM175* are important predictors of SR and pattern of spread, with high levels of expression in top seed regions such as substantia nigra. *GBA* encodes the lysosomal protein glucocerebrosidase, which has been implicated in Parkinson's disease pathogenesis by multiple experimental approaches in addition to GWAS. Both levels and activity of glucocerebrosidase are decreased in Parkinson's disease patients, with the most pronounced effects occurring in substantia nigra (Gegg *et al.*, 2012). Loss of function mutations affecting GBA enzymatic activity interfere with lysosomal protein degradation, leading to α-synuclein accumulation and neurodegeneration in animal models (Mazzulli *et al.*, 2011). Decreased levels of GBA also enhance intercellular transmission of α-synuclein (Bae *et al.*, 2014), suggesting that transcription of *GBA* can contribute to both initiation and spread of Parkinson's disease pathology.

TMEM175 is a lysosomal K^+ channel, serving as the primary lysosomal K^+ conductance, with major roles in maintaining the lysosomal pH gradient and regulating lysosome fusion with other organelles (Cang *et al.*, 2015). Mutations of *TMEM175* have been shown to decrease glucocerebrosidase activity by destabilizing lysosomal pH, leading to α-synuclein accumulation (Jinn *et al.*, 2017). GBA and TMEM175 therefore represent two lysosomal proteins in the same potential mechanistic pathway, positioned to modulate early α-synuclein-related pathology. Interestingly, *SNCA* expression itself does not predict SR or regional atrophy, in accordance with other results (Freeze *et al.*, 2018). This may suggest that levels of α-synuclein are less important than pathways that promote the stochastic production of even small amounts of pathological species, which may then increase in concentration by prion-like templating and aggregation mechanisms (Iljina *et al.*, 2016), possibly involving dysfunctional lysosomal processing.

Increased expression of Parkinson's disease immune-related genes also predicts SR and spread pattern. One of these genes, *IL1R2*, is a complex regulator of IL1-mediated inflammation (McMahan *et al.*, 1991; Lang *et al.*, 1998). Intriguingly, two MHCII genes also predict SR, including *HLA-DQA1,* which plays an important role in antigen presentation. As microglia are the primary antigen presenting cells in the brain (Hickey and Kimura, 1988), we sought to determine whether microglia are enriched in likely seed regions. Indeed, microglial high fidelity gene expression shows increased microglia abundance in likely seed regions. This finding is concordant with neuropathological studies in normal subjects showing larger numbers of microglia in areas related to Parkinson's disease pathology. For instance in humans, substantia nigra, putamen and pallidum contain ~2-fold more microglia than frontal grey matter (Mittelbronn *et al.*, 2001). The relative

distribution of microglia is similar in mice, suggesting that anatomic variability in microglial density may be conserved across species. As in humans, substantia nigra, putamen and pallidum also contain ~2-fold more microglia than cortical grey matter (Lawson *et al.*, 1990). Although regional enrichment of microglia in normal brains does not prove that such regions are more susceptible to microglia mediated pathology in Parkinson's disease, there is correspondence between areas of high microglial density in Parkinson's disease patients. For example, histopathological analysis has shown that the substantia nigra in Parkinson's disease subjects contains 4-fold more activated microglia than cortical regions (Imamura *et al.*, 2003). Improved imaging of different microglial species *in vivo* may provide insight into the relationship between baseline numbers of microglia and activated subtypes in Parkinson's disease. Further work on high fidelity gene expression may also allow resolution of these subtypes in Parkinson's disease patients by transcriptomic methods, an area of active investigation.

It is possible that microglia-mediated pathology may require additional disease initiation events, such as accumulation of pathological α-synuclein species. Microglia have been shown to interact with α-synuclein in numerous studies. For instance, α-synuclein acts as a microglial chemoattractant (Wang *et al.*, 2015) and α-synuclein aggregates trigger a microglial pro-inflammatory response that causes neuronal toxicity (Zhang *et al.*, 2005). Together our findings suggest a model in which early pathology sites are vulnerable to dysfunctional lysosomal α-synuclein processing as well as microglia mediated neuroinflammation that may directly cause neuronal damage and also promote α-synuclein spread, similar to the spread of tau in Alzheimer disease (Asai *et al.*, 2015).

We emphasize that our findings primarily relate to disease initiation and patterning of early disease spread, with connectivity patterns playing a critical role in determining the overall atrophy map as disease progresses throughout the brain. Other local factors may also play an important role in determining the regional pattern of disease, although findings from our own group suggest that trans-synaptic models of disease spread are more predictive than purely distance-based spread models (Pandya *et al.* 2019). As posited by other groups, there may be cell-type specific vulnerability to α-synuclein pathology, or other types of pathological insult mediated by the immune system. Downstream effects from cell death in connected regions may also be relevant. For example, the striatum is affected by substantia nigra pathology not only due to transmission of pathological α-synuclein, but also by dopamine deprivation itself.

There are several limitations of this study that warrant discussion. We use MRI-derived atrophy as a marker of regional neurodegeneration. This provides a measure of local effective pathology, as regional atrophy largely reflects neurodegeneration in the form of cellular atrophy and death. For instance, substantia nigra dopaminergic cell death has been shown to correlate with disease duration and progression of neurodegeneration (Damier *et al.*, 1999). In mice and non-human primates, substantia nigra injection of human Lewy body extracts induces progressive death of substantia nigra dopaminergic neurons and concomitant reduction in striatal dopaminergic terminals (Recasens *et al.*, 2014), suggesting that there is a close relationship between cell death and α-synuclein pathology. Indeed, highly atrophic top seed regions in this study, such as substantia nigra and amygdala, have been shown to exhibit Lewy pathology in all patients in a cohort studied by Jellinger (2003). However, we acknowledge that there are regions in which Lewy pathology can frequently occur without marked atrophy on MRI. For instance, cingulate cortex exhibits Lewy pathology in 34% of patients in the same study, and yet is not significantly atrophic in our dataset. Certain brain regions may be more resistant to α-synuclein pathology, possibly due to cell-type specific mechanisms. Further research in this area is likely to provide important insight into additional mechanisms that control the regional pattern of disease.

We used a DBM approach to quantifying regional atrophy on a 78 region parcellation of the brain. Although some other commonly used parcellations contain more brain regions, we chose to sacrifice some spatial resolution for improved signal to noise ratio in the atrophy map, which was derived from a large PPMI Parkinson's disease subject cohort. The high precision of the atrophy map is relevant, as conflicting results in other studies may be in part due to lack of statistical power and precision. For example, while substantia nigra volumetric change in Parkinson's disease has been analysed in several other studies, there have been discrepant results. While some groups have reported volume loss, others have reported no change (Péran *et al.*, 2010) or even increased volume of the substantia nigra (Kwon *et al.*, 2012). Our study is notable for containing many more subjects (232) than the studies by Péran *et al.* (30 subjects) and Kwon *et al.* (10 subjects); suggesting that this may be an important consideration in addition to other methodological differences.

Although DBM has been shown to be more sensitive to subcortical atrophy in other work (Scanlon *et al.*, 2011), it remains difficult to determine atrophy in the brainstem and certain other brain regions due to technical limitations of MRI including lack of spatial resolution and tissue contrast. Such regions include olfactory cortex and brainstem structures such as the dorsal motor nucleus of the vagus nerve and locus coeruleus, which have been posited to serve as early pathology sites in Parkinson's disease (Braak *et al.*, 2003). Olfactory cortex and the dorsal motor nucleus of the vagus nerve specifically have also been suggested to act as accumulation sites for extra-CNS α-synuclein transmitted by cranial nerve I and visceral afferents. While our findings cannot address these claims, in the future these structures may be more amenable to analysis with improved atlas construction (Bianciardi *et al.*, 2015) and T_2* imaging at high field strength. Even if there are additional early sites of disease, we suggest that the top seed

regions in this study likely still serve as important mediators of the regional atrophy pattern; possibly by accumulating subthreshold levels of pathology from other connected early disease sites.

In this study we used gene expression data derived from a relatively small number of healthy control subjects. The creation of the Allen Brain Atlas was extremely resource intensive, and a similar dedicated gene expression atlas for Parkinson's disease subjects is not yet available. There may be differences in Parkinson's disease and healthy control regional transcription that we cannot address with our current approach, but this will likely be a fruitful area of future research. We also note that our analysis of genetic factors is limited to transcript abundance. Although this is an informative measure, protein levels may not scale linearly with transcript abundance. Importantly, protein levels and activity are known to often be more relevant to cellular function. Additional factors such as protein folding, post-translational modification, and subcellular localization and trafficking, are also highly relevant to the ultimate impact of gene expression on cellular dynamics. These reasons may explain why autophagy-related and mitochondrial gene expression does not predict SR and pattern of spread, despite evidence for their importance from GWAS. Advances in proteomics may provide further insight into these issues, although most of this work is currently being performed in model organisms (Sharma *et al.*, 2015).

In summary, we demonstrate that lysosomal and immune-related molecular pathways are likely critical contributors to Parkinson's disease initiation and early disease propagation, and may be particularly relevant in designing disease-modifying treatments that are not reliant on dopamine replacement or ablation/DBS-based circuit modulation. Importantly, we are able to deduce these genetic effects from non-invasive MRI and computational analysis, which may facilitate future development of combined genetic/imaging biomarkers. Further work on techniques to image various α-synuclein species, and microglial distribution and activity, may provide further insight into early disease states.

Acknowledgements

PPMI—a public-private partnership—is funded by the Michael J. Fox Foundation for Parkinson's Research funding partners Abbvie, Avid Radiopharmaceuticals, Biogen Idec, BioLegend, Bristol-Myers Squibb, Eli Lilly & Co., F. Hoffman-La Roche, Ltd., GE Healthcare, Genentech, GlaxoSmithKline, Lundbeck, Merck, MesoScale Discovery, Piramal, Pfizer, Sanofi Genzyme, Servier, Takeda, Teva, and UCB.

Funding

Radiological Society of North America (RSNA) resident research grant RR1813 (B.F.).

Competing interests

The authors report no competing interests.

Supplementary material

Supplementary material is available at *Brain* online.

References

Asai H, Ikezu S, Tsunoda S, Medalla M, Luebke J, Haydar T, et al. Depletion of microglia and inhibition of exosome synthesis halt tau propagation. Nat Neurosci 2015; 18: 1584–93.

Ashburner J, Hutton C, Frackowiak R, Johnsrude I, Price C, Friston K. Identifying global anatomical differences: deformation-based morphometry. Hum Brain Mapp 1998; 6: 348–57.

Bae E-J, Yang N-Y, Song M, Lee CS, Lee JS, Jung BC, et al. Glucocerebrosidase depletion enhances cell-to-cell transmission of α-synuclein. Nat Commun 2014; 5: 4755.

Bar-Joseph Z, Gifford DK, Jaakkola TS. Fast optimal leaf ordering for hierarchical clustering. Bioinformatics 2001; 17: S22–9.

Bhattacharya S, Dunn P, Thomas CG, Smith B, Schaefer H, Chen J, et al. ImmPort, toward repurposing of open access immunological assay data for translational and clinical research. Sci Data 2018; 5: 180015.

Bianciardi M, Toschi N, Edlow BL, Eichner C, Setsompop K, Polimeni JR, et al. Toward an in vivo neuroimaging template of human brainstem nuclei of the ascending arousal, autonomic, and motor systems. Brain Connect 2015; 5: 597–607.

Braak H, Del Tredici K, Rüb U, de Vos RA, Jansen Steur EN, Braak E. Staging of brain pathology related to sporadic Parkinson's disease. Neurobiol Aging 2003; 24: 197–211.

Cang C, Aranda K, Seo Y, Gasnier B, Ren D. TMEM175 is an organelle K(+) channel regulating lysosomal function. Cell 2015; 162: 1101–12.

Chang D, Nalls MA, Hallgrímsdóttir IB, Hunkapiller J, van der Brug M, Cai F, et al. A meta-analysis of genome-wide association studies identifies 17 new Parkinson's disease risk loci. Nat Genet 2017; 49: 1511–6.

Chaudhuri KR, Healy DG, Schapira AH. Non-motor symptoms of Parkinson's disease: diagnosis and management. Lancet Neurol 2006; 5: 235–45.

Damier P, Hirsch EC, Agid Y, Graybiel AM. The substantia nigra of the human brain. II. Patterns of loss of dopamine-containing neurons in Parkinson's disease. Brain 1999; 122: 1437–48.

Desplats P, Lee H-J, Bae E-J, Patrick C, Rockenstein E, Crews L, et al. Inclusion formation and neuronal cell death through neuron-to-neuron transmission of α-synuclein. Proc Natl Acad Sci 2009; 106: 13010–5.

Freeze B, Acosta D, Pandya S, Zhao Y, Raj A. Regional expression of genes mediating trans-synaptic alpha-synuclein transfer predicts regional atrophy in Parkinson disease. NeuroImage Clin 2018; 18: 456–66.

Gegg ME, Burke D, Heales SJR, Cooper JM, Hardy J, Wood NW, et al. Glucocerebrosidase deficiency in substantia nigra of Parkinson disease brains. Ann Neurol 2012; 72: 455–63.

Hastie T. Statistical learning with sparsity. Chapman and Hall/CRC; 2015. Available from: https://www.taylorfrancis.com/books/9781498712170.

Hawrylycz M, Miller JA, Menon V, Feng D, Dolbeare T, Guillozet-Bongaarts AL, et al. Canonical genetic signatures of the adult human brain. Nat Neurosci 2015; 18: 1832–44.

Hawrylycz MJ, Lein ES, Guillozet-Bongaarts AL, Shen EH, Ng L, Miller JA, et al. An anatomically comprehensive atlas of the adult human brain transcriptome. Nature 2012; 489: 391–9.

Hickey WF, Kimura H. Perivascular microglial cells of the CNS are bone marrow-derived and present antigen in vivo. Science 1988; 239: 290–2.

Iljina M, Garcia GA, Horrocks MH, Tosatto L, Choi ML, Ganzinger KA, et al. Kinetic model of the aggregation of alpha-synuclein provides insights into prion-like spreading. Proc Natl Acad Sci 2016; 113: E1206–15.

Imamura K, Hishikawa N, Sawada M, Nagatsu T, Yoshida M, Hashizume Y. Distribution of major histocompatibility complex class II-positive microglia and cytokine profile of Parkinson's disease brains. Acta Neuropathol 2003; 106: 518–26.

Iturria-Medina Y, Canales-Rodríguez EJ, Melie-García L, Valdés-Hernández PA, Martínez-Montes E, Alemán-Gómez Y, et al. Characterizing brain anatomical connections using diffusion weighted MRI and graph theory. Neuroimage 2007; 36: 645–60.

Jellinger KA. Alpha-synuclein pathology in Parkinson's and Alzheimer's disease brain: incidence and topographic distribution: a pilot study. Acta Neuropathol 2003; 106: 191–201.

Jia X, Liang P, Li Y, Shi L, Wang D, Li K. Longitudinal study of gray matter changes in Parkinson disease. Am. J. Neuroradiol 2015; 36: 2219–26.

Jinn S, Drolet RE, Cramer PE, Wong AHK, Toolan DM, Gretzula CA, et al. TMEM175 deficiency impairs lysosomal and mitochondrial function and increases α-synuclein aggregation. Proc Natl Acad Sci 2017; 114: 2389–94.

Kelley KW, Nakao-Inoue H, Molofsky A V., Oldham MC. Variation among intact tissue samples reveals the core transcriptional features of human CNS cell classes. Nat Neurosci 2018; 21: 1171–84.

Kowal SL, Dall TM, Chakrabarti R, Storm MV, Jain A. The current and projected economic burden of Parkinson's disease in the United States. Mov Disord 2013; 28: 311–8.

Kwon D-H, Kim J-M, Oh S-H, Jeong H-J, Park S-Y, Oh E-S, et al. Seven-Tesla magnetic resonance images of the substantia nigra in Parkinson disease. Ann Neurol 2012; 71: 267–77.

Lang D, Knop J, Wesche H, Raffetseder U, Kurrle R, Boraschi D, et al. The type II IL-1 receptor interacts with the IL-1 receptor accessory protein: a novel mechanism of regulation of IL-1 responsiveness. J Immunol 1998; 161: 6871–7.

Lawson LJ, Perry VH, Dri P, Gordon S. Heterogeneity in the distribution and morphology of microglia in the normal adult mouse brain. Neuroscience 1990; 39: 151–70.

Luk KC, Kehm VM, Zhang B, O'Brien P, Trojanowski JQ, Lee VMY. Intracerebral inoculation of pathological α-synuclein initiates a rapidly progressive neurodegenerative α-synucleinopathy in mice. J Exp Med 2012; 209: 975–86.

Mao X, Ou MT, Karuppagounder SS, Kam T-I, Yin X, Xiong Y, et al. Pathological α-synuclein transmission initiated by binding lymphocyte-activation gene 3. Science 2016; 353: aah3374.

Marek K, Jennings D, Lasch S, Siderowf A, Tanner C, Simuni T, et al. The Parkinson progression marker initiative (PPMI). Prog Neurobiol 2011; 95: 629–35.

Mazzulli JR, Xu Y-H, Sun Y, Knight AL, McLean PJ, Caldwell GA, et al. Gaucher disease glucocerebrosidase and α-synuclein form a bidirectional pathogenic loop in synucleinopathies. Cell 2011; 146: 37–52.

McMahan CJ, Slack JL, Mosley B, Cosman D, Lupton SD, Brunton LL, et al. A novel IL-1 receptor, cloned from B cells by mammalian expression, is expressed in many cell types. EMBO J 1991; 10: 2821–32.

Mittelbronn M, Dietz K, Schluesener HJ, Meyermann R. Local distribution of microglia in the normal adult human central nervous system differs by up to one order of magnitude. Acta Neuropathol 2001; 101: 249–55.

Pandya S, Zeighami Y, Freeze B, Dadar M, Collins L, Dagher A, Raj A. Predictive model of spread of Parkinson's pathology using network diffusion. Neuroimage 2019; 192: 178–94.

Péran P, Cherubini A, Assogna F, Piras F, Quattrocchi C, Peppe A, et al. Magnetic resonance imaging markers of Parkinson's disease nigrostriatal signature. Brain 2010; 133: 3423–33.

Raj A, Kuceyeski A, Weiner M. A network diffusion model of disease progression in dementia. Neuron 2012; 73: 1204–15.

Recasens A, Dehay B, Bové J, Carballo-Carbajal I, Dovero S, Pérez-Villalba A, et al. Lewy body extracts from Parkinson disease brains trigger α-synuclein pathology and neurodegeneration in mice and monkeys. Ann Neurol 2014; 75: 351–62.

Scanlon C, Mueller SG, Tosun D, Cheong I, Garcia P, Barakos J, et al. Impact of methodologic choice for automatic detection of different aspects of brain atrophy by using temporal lobe epilepsy as a model. Am J Neuroradiol 2011; 32: 1669–76.

Sharma K, Schmitt S, Bergner CG, Tyanova S, Kannaiyan N, Manrique-Hoyos N, et al. Cell type- and brain region-resolved mouse brain proteome. Nat Neurosci 2015; 18: 1819–31.

Tibshirani R. Regression shrinkage and selection via the lasso: a retrospective. J R Stat Soc Series B Stat Methodol 2011; 73: 273–82.

Tinaz S, Courtney MG, Stern CE. Focal cortical and subcortical atrophy in early Parkinson's disease. Mov Disord 2011; 26: 436–41.

Torok J, Maia PD, Powell F, Pandya S, Raj A. A method for inferring regional origins of neurodegeneration. Brain 2018; 141: 863–76.

Wang S, Chu C-H, Stewart T, Ginghina C, Wang Y, Nie H, et al. α-Synuclein, a chemoattractant, directs microglial migration via H_2O_2-dependent Lyn phosphorylation. Proc Natl Acad Sci 2015; 112: E1926–35.

Yau Y, Zeighami Y, Baker TE, Larcher K, Vainik U, Dadar M, et al. Network connectivity determines cortical thinning in early Parkinson's disease progression. Nat Commun 2018; 9: 12.

Zeighami Y, Ulla M, Iturria-Medina Y, Dadar M, Zhang Y, Larcher KM-H, et al. Network structure of brain atrophy in de novo Parkinson's disease. Elife 2015; 4. Available from: https://elifesciences.org/articles/08440.

Zhang W, Wang T, Pei Z, Miller DS, Wu X, Block ML, et al. Aggregated α-synuclein activates microglia: a process leading to disease progression in Parkinson's disease. FASEB J 2005; 19: 533–42.